Author(s): Mammen, Nisha; Malola, Sami; Honkala, Karoliina; Häkkinen, Hannu

Title: Selective Acrolein Hydrogenation over Ligand-Protected Gold Clusters : A Venus Flytrap Mechanism

Year: 2022

Version: Published version

Selective Acrolein Hydrogenation over Ligand-Protected Gold Clusters: A Venus Flytrap Mechanism

Nisha Mammen, Sami Malola, Karoliina Honkala, and Hannu Häkkinen*

ACCESS | Metrics & More | Article Recommendations | Supporting Information

ABSTRACT: The catalytic partial hydrogenation of α,β-unsaturated aldehydes is an ideal reaction to understand the selectivity between two different functional groups Here the two functional groups are C═C and C═O, and the hydrogenation of C═O is preferentially desired due to the importance of the issuing products, unsaturated alcohols, in fine-chemical industries. Using density functional theory calculations, we investigate the catalytic competency toward this reaction of a Au nanocluster in the presence of protecting ligands that offer higher stability and the possibility for the uniform distribution of size-selected clusters in the catalytic system. *meta*-Mercaptobenzoic-acid-protected-protected Au clusters exhibit special (bidentate) ligand−metal interactions: two weak interactions, O═C−OH···Au and Ph-(π)···Au, in addition to the strong S−Au covalent bonds. We find that Ph(π)···Au interactions break (or open) to expose unprotected, low-coordinated Au sites on the cluster, which have a high propensity for trapping incoming reactant molecules. We study the partial hydrogenation of acrolein at these sites and find that the unsaturated alcohol, 1-propenol, is selectively favored over possible products. The opening of the π···Au interaction and the trapping of reactant molecules at Au sites are similar to a Venus flytrap mechanism where the flowers in the plant exhibit motion to actively trap its prey.

KEYWORDS: *monolayer-protected clusters, acrolein reduction, catalysis, gold, nanoclusters, density functional theory*
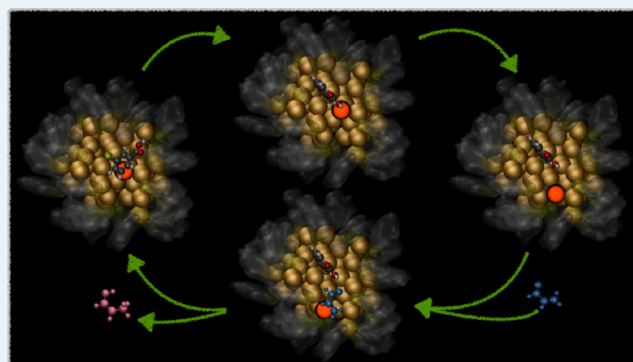
INTRODUCTION

Studies in the field of catalysis are driven by the search for new or improved catalytic materials that are cheaper or offer higher stability, lower activation barriers, and/or higher selectivity to the desired products in a catalytic process, as compared with presently used catalysts. Even a small percentage improvement in any of these qualities translates to a more efficient and economical use of energy and natural resources.

Several of the biomass-derived molecules that are important in chemical industries have multiple functional groups. It is crucial to gain a coherent sense of how one can selectively react upon one type of functional group over another. As an example, the selective hydrogenation of α,β-unsaturated aldehydes is a model reaction to understand the selectivity between C═C and C═O groups. The selective hydrogenation of the C═O bond leads to the formation of an unsaturated (allyl) alcohol. This is an intermediary reaction that is important in industries that deal with fine chemicals such as perfumes, flavoring agents, and pharmaceuticals, and hence it is desired over the hydrogenation of the C═C bond.[1,2]

In this study, we investigate the partial hydrogenation of acrolein, which is the smallest molecule with both C═C and C═O bonds. Scheme 1 shows the competing reaction pathways

Scheme 1. Partial Hydrogenation of Acrolein to Give Three Possible Products: Propanal, 1-Propenol, and 2-Propenol
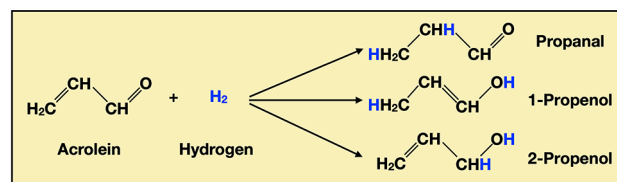
to form three different products: propanal (H atoms added to C3 and C2), 1-propenol (H atoms added to O and C3), and 2-propenol (H atoms added to O and C1). (The C atoms in the acrolein molecule are numbered 1−3 starting from the O-end to the C-end of the molecule.) The saturated aldehyde, propanal, is the thermodynamically favored product, and 1-propenol

tautomerizes to propanal over time. As a consequence, to achieve the target product, that is, 2-propenol, one requires control over the thermodynamics of the reaction intermediates or the kinetics of the competing processes offered by the appropriate catalyst.

Different metal surfaces and bimetallic systems have been shown, using experimental methods and density functional theory (DFT) calculations, to have specific selectivities to unsaturated alcohols based on effects due to the size, the electron density, the steric hindrance, the presence of promoter or inhibitor atoms, or the nature of the solvent.[1−9] The hydrogenation of the C=O bond in acrolein has been shown to be highly active and selective on Pd(111) surfaces when they are covered with ligand-like oxopropyl spectator species. This leads to a ligand-assisted promotion of the desired reaction pathway,[10−12] suggesting that ligand-covered metal surfaces can also perform as excellent catalysts for this reaction. Nanometer-sized Au particles (without ligands) have also been shown to be catalytically active and selective toward the formation of unsaturated alcohols; the dependence of the activity and the selectivity on the size of the particle and the nature of the oxide support has been studied.[13−19]

With the knowledge that catalytic properties are highly sensitive to the size of a nanocluster and that the addition or removal of a single atom could lead to loss of its catalytic properties, efforts are now focused on the study of atomically precise nanoclusters. There are, however, challenges to be met pertaining to the instability of these clusters due to their tendency to aggregate into larger particles and having precise control over a uniform size distribution of clusters to be used in applications. Toward this purpose, several methods have been suggested: (i) confining clusters in crystalline zeolite-type cages,[20] (ii) sorting monodisperse metal clusters by mass spectrometry and then soft-landing them onto supports,[21−23] and (iii) stabilizing/capping clusters using a monolayer of organic ligands and removing these ligands by treatments after the clusters are anchored to the supports.[24−29] The supported clusters generated by methods (ii) and (iii) may still be prone, however, to sintering and form larger sized clusters under reaction conditions.

In this study, we focus on monolayer-protected atomically precise clusters and investigate their catalytic competency without the removal of ligands and in the absence of a support. Recent reports with combined theoretical and experimental data have shown that these clusters can catalyze reactions in solution such as the cycloisomerization of alkynyl amine, the hydration of alkynes, and C−N bond formation in aniline carbonylation.[30−32] Experimental electrospray ionization−mass and nuclear magnetic resonance spectra before and after the catalytic reactions confirm that the clusters retain their ligands after the reaction; that is, the reaction mechanism involves no removal of ligands. Ligands are chemically bonded to the metal cluster, and hence they undoubtedly affect the catalytic properties.[33] For example, increasing the chain length and reducing the packing density of thiolated polyethylene glycol ligands on Au clusters have been shown to improve the catalytic activity of the clusters toward the reduction of 4-nitrophenol.[34] The chemoselectivity toward the hydrogenation of cinnamaldehyde by FePt bimetallic nanoparticles stabilized with carboxylate ligands was significantly altered upon changing the chain length or the electron-withdrawing capability of the ligands.[35] In addition, ligands can also determine the solubility of the cluster in its environment[36] and affect the optical properties by imposing chirality that may

bring about possibilities for stereoselective catalysis.[37,38] Whereas most of the studies showing the catalytic activity of these clusters are experimental in nature, there is very little clarity on the atomistic picture of the catalytic mechanisms and the role of the ligands in the process. Some examples of computational research in this area include the report on the mechanism of the electrocatalytic reduction of CO_2 on $Cu_{32}H_{20}L_{12}$ (L = dithiophosphate ligand) clusters that was determined using a combination of experiments and DFT calculations.[39] In a previous work done by us, we reported a single-site mechanism for the reduction of ketones to alcohols on $Cu_{25}H_{10}L_{18}$ (L = $SPhCl_2$), which was confirmed by experiments.[40] Au clusters protected by secondary phosphine oxides were also shown to exhibit a cooperative effect at the metal−ligand interface that enabled the heterolytic dissociation of H_2 and the selective hydrogenation of aldehydes and ketones to corresponding alcohols.[41,42]

The catalyst in this study is a *meta*-mercaptobenzoic acid (*m*-MBA)-protected Au_{68} cluster. It is a water-soluble cluster that has been used to design cluster-marker hybrids for tracking proteins in live cells due to their high reactivity toward biomolecules.[43,44] The structure of the *m*-MBA-protected Au_{68} cluster was determined (in 2014) using low-dose electron microscopy techniques and 3D image reconstruction.[45]

The distinct chemistry in the ligand layer of $Au_{68}(m\text{-MBA})_{32}$ was revealed in 2017 by a combination of experimental and computational techniques.[46,47] The presence of the *m*-MBA ligands brings about three unique interactions not observed in similar sized clusters or even the closely related *p*-MBA-protected clusters:[47,48] (i) COOH···COOH hydrogen bonding between two neighboring ligands as well as two new interactions at the ligand−gold interface, (ii) hydrogen-bond-like O=C−OH···Au and (iii) Ph(π)···Au when the ligand lies "flat" on the gold core. These interactions help to explain the lower ligand density and the higher reactivity toward thiol-modified DNA observed in the *m*-MBA clusters when compared with other clusters of similar sizes.[46] On the basis of this observed reactivity, it was suggested[47] that these clusters could potentially act as catalysts. The weak interactions at the metal−ligand interface could be sacrificed, exposing unprotected Au atoms that could then favorably bind incoming reactant molecules.

In 2020, we reported extensive molecular dynamics (MD) simulations[49] performed on these systems. We studied in detail the dynamic nature of these *m*-MBA ligands at 300 and 500 K and determined the thermodynamics and kinetics involved in the formation and breaking of the weak interactions at the ligand−metal interface. Between the two weak ligand−gold interactions, it is the π···Au interaction that is of particular interest in this study. Here we look into a scenario where the π···Au interaction is broken and the ligand is in an open position, leaving the Au atom unprotected. We show that this Au atom is highly under-coordinated, is mobile, and shows a propensity for binding reactant molecules such as hydrogen and acrolein. The ligands open to trap reactant molecules, similar to a Venus flytrap, where the flower can open and close its petals to trap its prey. We report the reaction pathways and barriers that lead to the formation of the three possible products of the partial hydrogenation of acrolein: propanal, 1-propenol, and 2-propenol. We find that the formation of the OH bond is selectively favored over the formation of the CH (C3−H) bond, and the most favored product is 1-propenol.

COMPUTATIONAL METHODS AND MODEL

We performed density functional theory (DFT) calculations as implemented in the GPAW package.[50] The wave functions were expanded on a real-space grid using the finite difference method with a grid spacing of ~0.2 Å. The generalized gradient approximation using the PBE (Perdew−Burke−Ernzerhof) formulation was used as the exchange-correlation functional.[51] Test calculations on other ligand-protected Au clusters have shown that including van der Waals corrections stabilizes the system by ~0.5 eV.[52] Detailed comparisons of the results of acrolein hydrogenation on surfaces with and without van der Waals corrections have shown that including these interactions does not alter the predicted reaction mechanism or the chemoselectivity of the catalyst.[5] We also provide our results from test calculations using the van der Waals correction proposed by Tkatchenko and Scheffler.[53] (See Table S2 of the Supporting Information.) Our results show that whereas the energies of the systems considered are lowered by 0.4 to 0.6 eV, the observed trends in adsorption energies at different sites and activation barriers for different steps in the reaction remain unaffected.

PBE functionals have been shown to exhibit quantitative discrepancies from experimental values of adsorption energies for noble gases and organic molecules on transition-metal surfaces.[54−56] However, they are highly successful in predicting trends in the stability, adsorption energies, and catalytic activity of different metal and metal oxide surfaces, as has been shown extensively by previous authors.[57−60] More importantly, these functionals have been shown to reliably describe the structural changes and interfacial chemistry brought about by the addition of thiolate ligands to the gold surface.[61] They have helped successfully verify the observed experimental crystal structures in several cases,[62−67] predict correct structures of the metallic core and the gold−thiolate interface, and describe structural transformations in these clusters involving isomerization and chiral inversion.[68,69]

A nonperiodic cubic cell large enough to include a ~6 Å vacuum in all six directions around the cluster was used in all calculations. For the study of the reactivity of the clusters at the site of the interest, where the $\pi\cdots$Au interaction was broken to expose the low-coordinated Au atom, only this highly reactive Au atom, six nearest-neighbor Au atoms, and adsorbate atoms were allowed to be free during the structural optimization until the forces on the atoms were <0.05 eV/Å. A Fermi−Dirac smearing of width 0.05 eV was used to improve the convergence.

The barriers for the different reaction steps and pathways in the reduction of acrolein on the cluster were determined using a combination of the climbing-image nudged elastic band method[70] and constrained minimization techniques.[71] Our estimates for the transition states obtained by constrained minimization methods were validated against those previously reported for the same reaction on different Au clusters to have similar bond lengths and geometries.[19]

Au$_{68}$(m-MBA)$_{32}$ is an asymmetric cluster with a metallic core of 68 Au atoms, ~1.4 nm in diameter, and 32 m-MBA thiolate ligands, making the total diameter of the cluster ~2.7 nm. The structure of the metal core was determined to atomic resolution using aberration-corrected transmission electron microscopy, performed with the use of a minimal electron dose and 3D image reconstruction.[45,46] This provided the coordinates for Au atoms in our DFT study. Because the structure for the ligand layer cannot be determined experimentally, the initial guess was

created using an in-house algorithm. It suggested several potential structural models taking into account both the sulfur−gold bonding at the ligand−metal interface and the steric constraints in the ligand layer.[47,72] The model structure thus generated was initialized using classical force-field simulations,[47] and validated using DFT and extensive (DFT-based) MD simulations.[49] We note that the ligand layers and surface Au atoms are highly dynamic, and the energy-configuration space of the system is marked with a multitude of local minima in energy. The computational expense of these calculations is brought about by the complexity of the system and reaction in addition to the large system size of ~560 atoms with ~2500 electrons. For high accuracy of the calculations, the wave functions are expanded in a cubic box of volume 38.4^3 Å^3 over a dense grid with spacing of 0.2 Å that accounts for 192 × 192 × 192 points in real space.

Figure 1a shows the energetically optimized structure of the cluster. We highlight an example of the $\pi\cdots$Au interaction
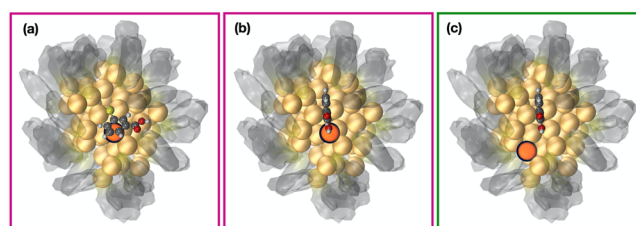

Figure 1. Ligands and surface Au atoms are highly dynamic. (a,b) Configurations of the system when a $\pi\cdots$Au interaction is closed and open, respectively. (b,c) Ligand in the open position, with two different positions for the Au atom (orange) marked. The relative energies of the structures in panels a−c are −0.22, 0.16, and 0.00 eV, respectively. Only one ligand is highlighted to show the site of interest, whereas the rest of the 32 ligands are shown as a (transparent) gray surface and are fixed in all calculations. The atoms S, C, O, and H in the highlighted ligand are shown in yellow, gray, red, and white, respectively. All Au atoms in the cluster are shown in gold, except for the one protected/unprotected mobile Au atom colored orange. The colors of the boxes, magenta and green, refer to this Au atom in positions P1 and P2, respectively.

between the phenyl ring of one ligand and a Au atom colored orange. The distance between the Au atom and the center of the phenyl ring is 3.06 Å. When this ligand moves away from the Au atom, it optimizes to the structure in Figure 1b, which is 0.38 eV higher in energy than the structure in Figure 1a. In our previous work, we had computed the barrier to break this interaction to be 1.10 eV.[49]

We calculated the gas-phase reaction energies for the three pathways shown in Scheme 1. The hydrogenation of C=C, forming propanal, and that of C=O, forming allyl alcohol, have reaction energies of −1.64 and −0.95 eV, respectively. The formation of 1-propenol, by the addition of H atoms to the O- and C-ends of the acrolein, has a reaction energy of −1.29 eV. In an isolated acrolein molecule, the bond distances along the backbone are $d(O−C1) = 1.22$ Å, $d(C1−C2) = 1.48$ Å, and $d(C2−C3) = 1.34$ Å

The adsorption energies, E_{ads}, for H$_2$ and the acrolein molecule on the cluster are calculated using the equation

$$E_{ads} = E_{X/cluster} - E_{X(g)} - E_{cluster} \qquad (1)$$

where the three terms on the right-hand side are the total energies from DFT for the following systems: (i) the molecule X adsorbed on the cluster, (ii) the isolated X molecule in the gas
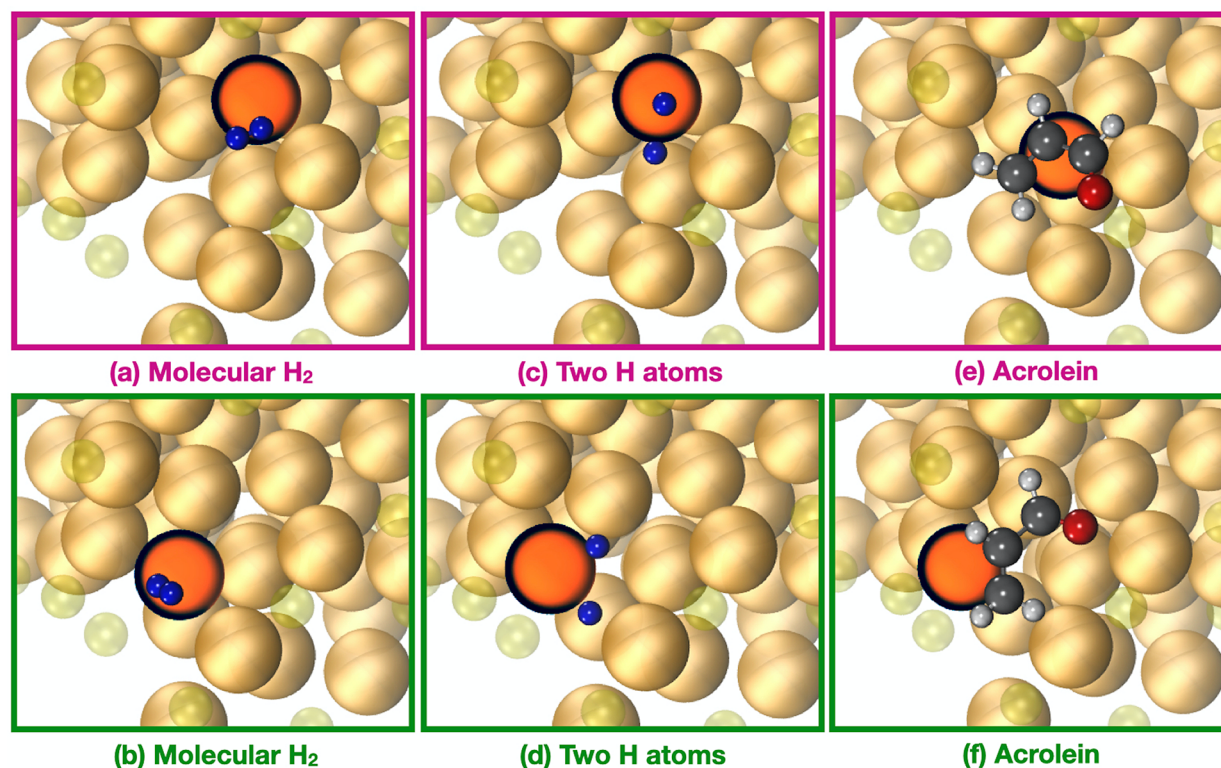
Figure 2. Optimized geometries of adsorbed (a,b) molecular H_2, (c,d) dissociated H_2, and (e,f) molecular acrolein. The reactive Au atom (orange) is in the P1 position in panels a, c, and e and in the P2 position in panels b, d, and f. The rest of the Au atoms are gold. H atoms from H_2 are blue, and those from acrolein are white. S, C, and O atoms are yellow (transparent), gray, and red, respectively. Only S atoms of the ligands are shown for clarity.

Table 1. Adsorption Energies (E_{ads}) and Bond Distances for the Reactants, Intermediates, and Products Adsorbed on the Cluster $Au_{68}(m\text{-MBA})_{32}$ When the Low-Coordinated Au Atom Was in Position 1 (P1) and Position 2 (P2)

	E_{ads} (eV)		$d(O-C1)$ (Å)		$d(C1-C2)$ (Å)		$d(C2-C3)$ (Å)	
adsorbate	P1	P2	P1	P2	P1	P2	P1	P2
H_2 molecule	0.15	−0.03						
2 H atoms	0.46	0.18						
acrolein	0.07	−0.11	1.22	1.22	1.49	1.50	1.39	1.40
CH intermediate	−0.44	−0.78	1.23	1.22	1.48	1.49	1.51	1.51
OH intermediate		−0.93		1.34		1.37		1.44
propanal	−1.55	−1.76	1.21	1.22	1.50	1.50	1.52	1.52
1-propenol	−1.73	−2.06	1.36	1.34	1.35	1.40	1.50	1.51
2-propenol		−1.69		1.42		1.52		1.39

phase (X = H_2/acrolein (CH_2=CH−CH=O)), and (iii) the bare cluster in Figure 1c (to be discussed further below), respectively. Similarly, the adsorption energies for the intermediates and products are calculated using the equation

$$E_{ads} = E_{Y/cluster} - E_{H_2(g)} - E_{acrolein(g)} - E_{cluster} \quad (2)$$

where the four terms on the right-hand side are the total energies from DFT for the following systems: (i) the intermediate or product Y adsorbed on the cluster, (ii) the H_2 molecule, (iii) the acrolein molecule, and (iv) the cluster in Figure 1c.

■ RESULTS AND DISCUSSION

We present the results in four sections to discuss (i) the dynamic nature of the ligands and the surface Au atoms, (ii) the adsorption of reactant molecules and the dissociation of hydrogen, (iii) the formation of intermediates, and (iv) the formation of the three products.

Dynamic Ligands and Surface Au Atoms. We consider the scenario where the $\pi\cdots$Au is being formed and broken, as shown in Figure 1a,b. When the weak interaction is broken, we see that the Au (orange) atom that is left unprotected is highly mobile, and it finds another suitable position on the surface of the cluster, as shown in Figure 1c. Upon comparing the energies of the structures in Figure 1b and c, we find that the latter is lower in energy by 0.16 eV. We use this cluster as the reference for the bare cluster in this study henceforth. In the Supporting Information, we provide a movie to show the ligand density around the cluster, the opening of the $\pi\cdots$Au interaction, and the motion of the unprotected Au atom from position P1 to P2.

We also wish to bring to the attention of the reader the color of the boxes in Figure 1. We will be using the color magenta to indicate the position of the orange Au atom to be in the initially preferred location stabilized by the $\pi\cdots$Au interaction (P1) and the color green to indicate the new position of the orange Au atom (P2).
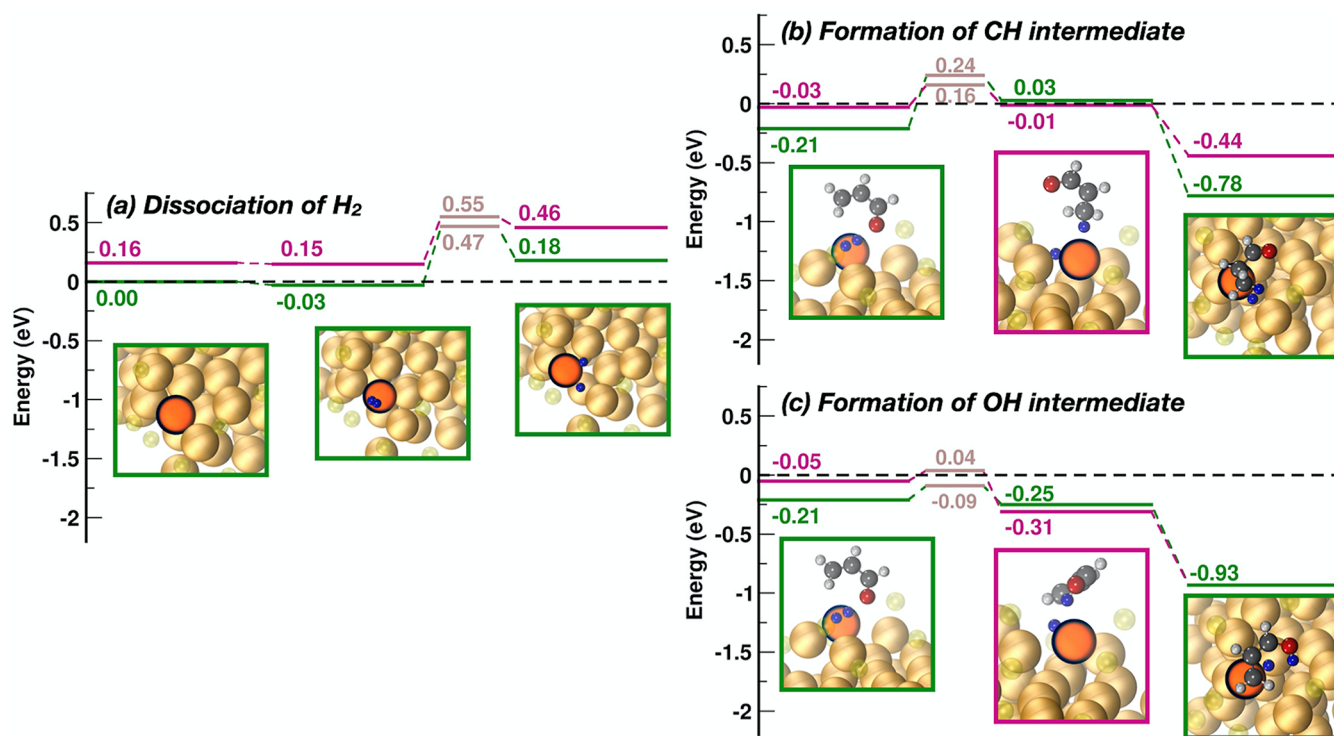
Figure 3. Energy pathways for the (a) dissociation of H$_2$, (b) formation of CH intermediate, and (c) formation of OH intermediate. The zero of energy is defined as $E_{cluster} + E_{H_2} + E_{acrolein} = 0$. The states marked in magenta and green refer to those with Au in positions P1 and P2, respectively, and the states marked in brown refer to the transition states. The colors used to represent the atoms in the insets are the same as those in Figure 2.

Adsorption of Hydrogen and Acrolein. Several initial geometries were considered for the adsorption of the reactant molecules, hydrogen and acrolein, on various sites of the cluster. However, in most cases, the molecules do not bind at all and move away from the cluster surface. In Figure 2, we show only the lowest energy geometries obtained for the adsorption of an H$_2$ molecule, two (dissociated) H atoms, and an acrolein molecule on the cluster at the unprotected Au (orange) atom when it is in the P1 and P2 positions. The values of E_{ads} for the adsorption geometries are listed in Table 1. We see that binding is more favorable with Au in the P2 position than the originally preferred $\pi\cdots$Au-interaction-stabilized P1 position. H$_2$ and acrolein molecules bind weakly to the cluster when the Au atom is in the P2 position, whereas the other configurations listed show endothermic binding. Previous authors (using Perdew–Wang PW91 functionals) have found the binding of acrolein to a Au$_{20}$ cluster (without ligands) to be exothermically favorable with $E_{ads} = -0.46$ eV.[19] The difference may be attributed to the presence of the ligands in our system.

In Figure 2a, the H$_2$ molecule is adsorbed horizontally on the reactive Au atom with $d(H-H) = 0.76$ Å and $d(H-Au) = 2.64$ and 2.91 Å. In Figure 2b, on the contrary, the H$_2$ is adsorbed (at an angle) atop the reactive Au atom with $d(H-H) = 0.75$ Å and $d(H-Au) = 2.92$ Å. The barrier for H$_2$ dissociation was estimated to be 0.40 and 0.50 eV for the two positions, P1 and P2, respectively. The same barrier on the Au(111) surface was found to be 1.45 eV[73], whereas on a naked Au$_{55}$ and a ligand-protected Au$_{55}$(Ph$_2$PO)$_{27}$ cluster, it was found to be 0.78 and 0.54 eV, respectively.[42] (The authors in ref 42 used PBE functionals with Grimme corrections for dispersion D2 terms, whereas in ref 73, they used revised PBE functionals with a modified version for the D2 terms.)

In Figure 2c,d, the dissociated H atoms are both bonded to the same Au atom with $d(H-H) = 1.98$ and 1.95 Å, respectively. The $d(H-Au)$ distances range between 1.58 and 1.69 Å. The homolytic dissociation of H$_2$ is endothermic by 0.31 and 0.21 eV at positions P1 and P2, respectively. This can be compared with values of 0.69 eV on the Au(111) surface[73] and 0.10 and 0.64 eV on a naked Au$_{55}$ and a protected Au$_{55}$(Ph$_2$PO)$_{27}$ cluster, respectively.[42] The energy pathways for the dissociation of H$_2$ at P1 (magenta) and P2 (green) sites are shown in Figure 3a.

In Figure 2e,f, the acrolein molecule binds to the Au atom via the C═C π-bond, that is, the C3 and C2 atoms of the molecule. In Figure 2e, $d(C3-Au) = 2.27$ Å and $d(C2-Au) = 2.32$ Å, whereas in Figure 2f, $d(C3-Au) = 2.22$ Å and $d(C2-Au) = 2.25$ Å.

Formation of Intermediates. Hydrogen is first adsorbed as a molecule on the reactive Au atom on the cluster and dissociates to two H atoms, as discussed in the previous section. Acrolein is then introduced to the system. Several initial geometries with different orientations of the molecule around the dissociated H atoms on Au atom at the P1 and P2 sites were considered. Two possible interactions between acrolein and the H atoms were investigated: The molecule could pick up one of the H atoms with the C-end of the molecule, forming the CH intermediate, or with the O-end of the molecule, forming the OH intermediate. The intermediate formed would then subsequently bind at the unprotected Au atom.

Figure 3b,c shows the energetics for the reaction pathways that lead to the formation of these intermediates. The energy barriers involved to pick up a dissociated H atom (break the H–Au bond) and form the CH bond are 0.19 and 0.45 eV when the Au atoms are at the P1 and P2 sites, respectively. The barriers to pick a H atom and form the OH bond, on the other hand, are 0.09 and 0.12 eV at the P1 and P2 sites, respectively. The two
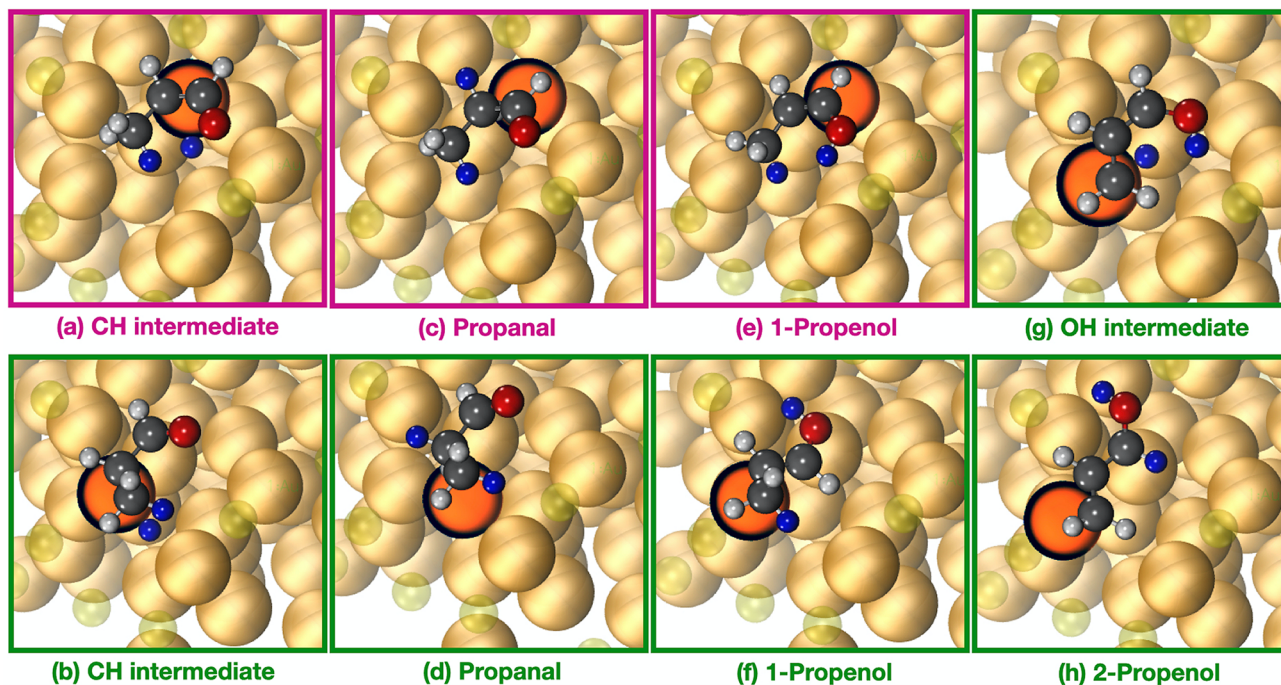
Figure 4. Optimized geometries of adsorbed (a,b) CH intermediate, (c,d) propanal, (e,f) 1-propenol, (g) OH intermediate, and (h) 2-propenol. The reactive Au atom (colored orange) is in the P1 position in panels a, c, and e and in the P2 position in panels b, d, and f−h. The colors used for the atoms are the same as those in Figure 2.
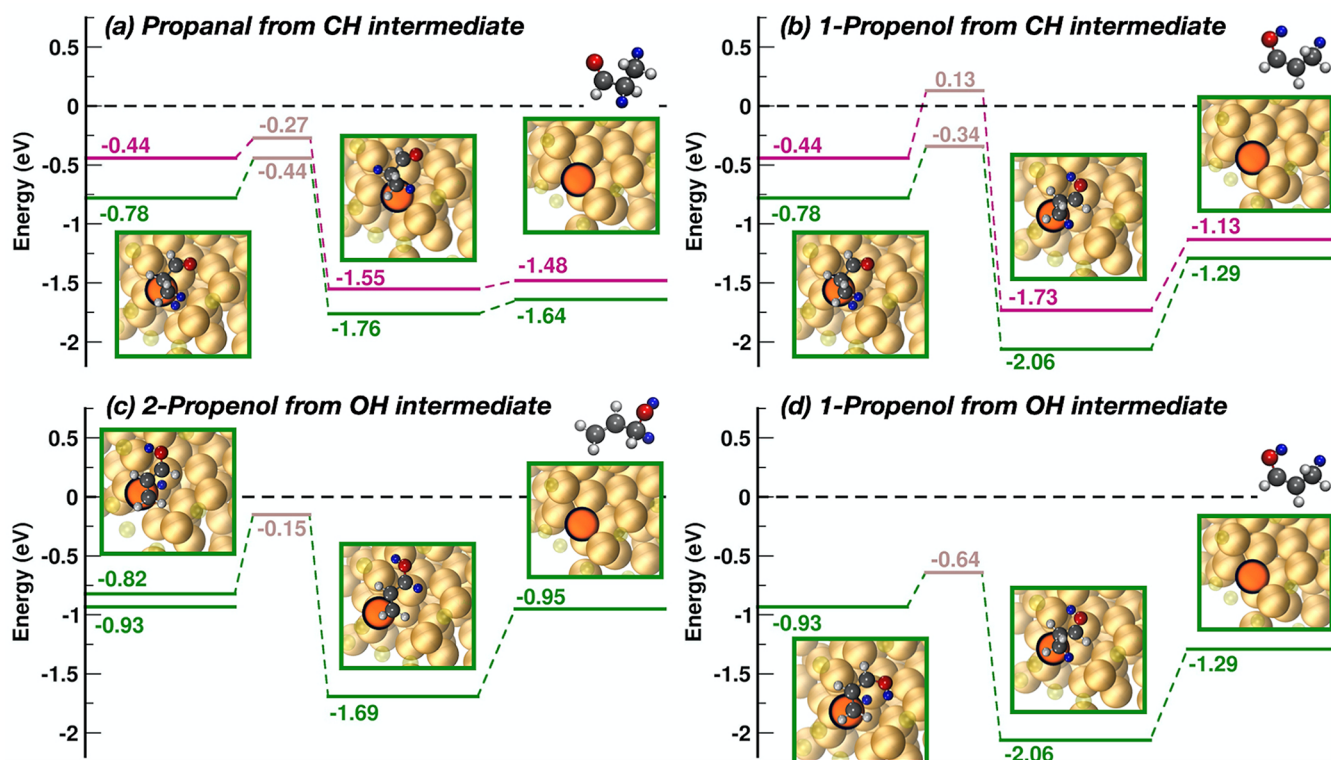

Figure 5. Energy pathways for the formation of (a) propanal and (b) 1-propenol, both from the CH intermediate, and (c) 2-propenol and (d) 1-propenol, both from the OH intermediate. The zero of energy is defined as $E_{H_2} + E_{acrolein} + E_{cluster} = 0$. The states marked in magenta and green refer to those with the Au in positions P1 and P2, respectively. The transition states and their relative energies are marked in brown. The colors used to represent the atoms in the insets are the same as those in Figure 2.

intermediates then bind exothermically at the Au atom on the cluster, forming C−Au bonds. We see that the energy of the system is highly sensitive to the orientation of the molecule with respect to the ligand layer and also to whether the molecule approaches the cluster surface via the O-end or the C-end.

Figure 4 shows the lowest energy geometries obtained for the two possible intermediate structures: the CH intermediate (see Figure 4a,b) and the OH intermediate (see Figure 4g). We see that the formation of the CH intermediate is possible at both sites P1 and P2. The binding at the P2 site is stronger than that at the P1 site (−0.78 vs −0.44 eV). After the formation of the CH bond, the C=C π-bond is now between the C2 and C1 atoms of the molecule; therefore, the intermediate binds to the Au atom via these two atoms. At P1, $d(C2-Au) = 2.26$ Å and $d(C1-Au) = 2.94$ Å, whereas at P2, $d(C2-Au) = 2.17$ Å and $d(C1-Au) = 2.87$ Å.

The formation of the OH intermediate, interestingly, is possible only at the P2 site. When the molecule approaches the Au atom at P1, the Au atom spontaneously (no energy barrier involved) moves to the P2 site to enable the adsorption of the OH intermediate with a binding strength of −0.93 eV. The formation of the OH intermediate does not affect the initial C=C π-bond between the C3 and C2 atoms of the molecule; therefore, it binds to the Au atom with $d(C3-Au) = 2.20$ Å and $d(C2-Au) = 3.07$ Å. Our results suggest that there is a clear thermodynamic driving force favoring the formation of the OH bond over the CH bond. The differences in the kinetic barriers involved are, however, quite small.

Formation of Products. Now, starting from these intermediates, we investigate four pathways leading to the three products. Consider the CH intermediate bound to the Au site. The second H atom bonded to the same Au can now move to either C2, forming propanal (see Figure 4c,d), or to O, forming 1-propenol (see Figure 4e,f). The product propanal does not bind to the Au atom any more due to the loss of the C=C (π) bond and lifts up from the cluster surface. 1-Propenol, however, weakly binds to the Au atom via C2=C1···Au.

The energy pathways for the formation of propanal and 1-propenol, respectively, from the CH intermediate are shown in Figure 5a,b. We see that the relative energies and barriers for the formation of propanal are lower (0.17 eV at P1 and 0.34 eV at P2) than those for the formation of 1-propenol (0.57 eV at P1 and 0.44 eV at P2), suggesting that propanal is the favored product once the CH intermediate is formed.

Similarly, now let us consider the OH intermediate bound to the orange Au atom. The second H atom can move either to C1 forming 2-propenol (see Figure 4h) or to C3 forming 1-propenol (see Figure 4f). Both unsaturated alcohols bind to the Au atom via the C=C π-bond. In the case of 2-propenol, the C=C is between C3 and C2 ($d(C3-Au) = 2.22$ Å and $d(C2-Au) = 2.27$ Å), whereas for 1-propenol, it is between the C2 and C1 atoms of the molecule ($d(C2-Au) = 2.21$ Å and $d(C1-Au) = 2.42$ Å).

Figure 5c,d shows the energy pathways for the formation of 2-propenol and 1-propenol, respectively, from the OH intermediate. This intermediate was found to be stable only with the Au at position P2. In Figure 5c, we see two initial states marked in green at −0.93 and −0.82 eV. The most stable configuration of the OH intermediate corresponds to the state with energy of −0.93 eV; however, we find that to facilitate the reaction, the system goes to a slightly higher energy (−0.82 eV) where the OH bond in the intermediate is oriented differently.

For the formation of products from the OH intermediate, on the basis of the energies of the structures and barriers involved (0.78 eV for 2-propenol vs 0.29 eV for 1-propenol), we see that 1-propenol is the thermodynamically and kinetically favored product. However, it is known that 1-propenol would eventually tautomerize to form propanal. This suggests that the Au$_{68}$(m-

MBA)$_{32}$ cluster is indeed a catalyst with low barriers for the reduction of acrolein; however, it may not exhibit a high selectivity for the formation of the desired allyl alcohol.

The details of each reaction step, including the reaction coordinates used and the bond distances between atoms at the initial, transition, and final states, are given in the Supporting Information. (See Table S1 and Figures S1 and S2.)

Most theoretical studies on the hydrogenation of acrolein do not consider the formation of 1-propenol.[19,42,74,75] They consider only the routes where H atoms are added to (i) C3 and C2 and (ii) O and C1. The 1-propenol, however, is formed by the addition of H atoms to C3 and O of the acrolein molecule. If we were to follow the same pattern as previous authors, then our results would suggest that the selectivity for the hydrogenation of the C=O bond would be higher than that of C=C. This is because we find that the OH intermediate is thermodynamically and kinetically more favorable than the CH intermediate. However, if we consider the formation of the 1-propenol by consecutively adding H atoms to C3 and O in either order, then we find that this is most favorable, which would eventually lead to the formation of propanal.

■ CONCLUSIONS

We have studied the catalytic activity of a Au nanocluster stabilized by *m*-MBA ligands using DFT calculations. On the basis of our results, we suggest that these clusters are highly stable and perform as a selective, mild-temperature (low-barrier) catalyst for the reduction of acrolein to an unsaturated alcohol (1-propenol) without the removal of any ligands. The ligands display a continuous motion, forming and breaking weak interactions between the ligand and the Au atoms on the cluster surface, which causes Au atoms on the cluster to be protected or unprotected. The cluster offers a unique reaction pathway for the catalytic mechanism. Understanding possible reaction mechanisms involved in such monolayer-protected clusters paves the path forward to designing better and more stable catalysts with chiral ligands that cause chiral selectivity for reactions with polyfunctional molecules. In addition, it brings about possibilities for recreating similar ligand−metal interfaces where ligands exhibit strong and weak interactions; the strong interactions provide stability to the cluster, whereas the weak interactions can be sacrificed to expose catalytically active sites on the surface.

■ ASSOCIATED CONTENT

ⓢ Supporting Information

The Supporting Information is available free of charge at https://pubs.acs.org/doi/10.1021/acscatal.1c04585.

■ AUTHOR INFORMATION

Corresponding Author

Hannu Häkkinen − *Department of Physics, Nanoscience Center, University of Jyväskylä, 40014 Jyväskylä, Finland; Department of Chemistry, Nanoscience Center, University of*

Jyväskylä, 40014 Jyväskylä, Finland; ◉ orcid.org/0000-0002-8558-5436; Email: hannu.j.hakkinen@jyu.fi

Authors

Nisha Mammen − *Department of Physics, Nanoscience Center, University of Jyväskylä, 40014 Jyväskylä, Finland;* ◉ orcid.org/0000-0002-1550-6333

Sami Malola − *Department of Physics, Nanoscience Center, University of Jyväskylä, 40014 Jyväskylä, Finland*

Karoliina Honkala − *Department of Chemistry, Nanoscience Center, University of Jyväskylä, 40014 Jyväskylä, Finland;* ◉ orcid.org/0000-0002-3166-1077

Complete contact information is available at:
https://pubs.acs.org/10.1021/acscatal.1c04585

Notes

The authors declare no competing financial interest.

■ REFERENCES

(1) Gallezot, P.; Richard, D. Selective Hydrogenation of α,β-Unsaturated Aldehydes. *Catal. Rev. - Sci. Eng.* **1998**, *40*, 81.

(2) Claus, P. Selective Hydrogenation of α,β-Unsaturated Aldehydes and Other C═O and C═C Bonds Containing Compounds. *Top. Catal.* **1998**, *5*, 51.

(3) Mäki-Arvela, P.; Hájek, J.; Salmi, T.; Murzin, D. Y. Chemoselective Hydrogenation of Carbonyl Compounds over Heterogeneous Catalysts. *Appl. Catal., A* **2005**, *292*, 1.

(4) Ponec, V. On the Role of Promoters in Hydrogenations on Metals; α,β-Unsaturated Aldehydes and Ketones. *Appl. Catal., A* **1997**, *149*, 27.

(5) Tuokko, S.; Pihko, P. M.; Honkala, K. First Principles Calculations for Hydrogenation of Acrolein on Pd and Pt: Chemoselectivity Depends on Steric Effects on the Surface. *Angew. Chem., Int. Ed.* **2016**, *128*, 1702.

(6) Hirschl, R.; Delbecq, F.; Sautet, P.; Hafner, J. Adsorption of unsaturated aldehydes on the (111) surface of a Pt−Fe alloy catalyst from first principles. *J. Catal.* **2003**, *217*, 354.

(7) Luneau, M.; Lim, J. S.; Patel, D. A.; Sykes, E. C. H.; Friend, C. M.; Sautet, P. Guidelines to Achieving High Selectivity for the Hydrogenation of α,β-Unsaturated Aldehydes with Bimetallic and Dilute Alloy Catalysts: A Review. *Chem. Rev.* **2020**, *120*, 12834.

(8) Loffreda, D.; Delbecq, F.; Vigné, F.; Sautet, P. Chemo-Regioselectivity in Heterogeneous Catalysis: Competitive Routes for C═O and C═C Hydrogenations from a Theoretical Approach. *J. Am. Chem. Soc.* **2006**, *128*, 1316.

(9) Loffreda, D.; Delbecq, F.; Vigné, F.; Sautet, P. Fast Prediction of Selectivity in Heterogeneous Catalysis from Extended Brønsted−Evans−Polanyi Relations: A Theoretical Insight. *Angew. Chemie. Int. Ed.* **2009**, *121*, 9140.

(10) Dostert, K.-H.; O'Brien, C. P.; Ivars-Barcelo, F.; Schauermann, S.; Freund, H.-J. Spectators Control Selectivity in Surface Chemistry: Acrolein Partial Hydrogenation Over Pd. *J. Am. Chem. Soc.* **2015**, *137*, 13496.

(11) Dostert, K.-H.; O'Brien, C. P.; Mirabella, F.; Ivars-Barcelo, F.; Attia, S.; Spadafora, E.; Schauermann, S.; Freund, H.-J. Selective Partial Hydrogenation of Acrolein on Pd: A Mechanistic Study. *ACS Catal.* **2017**, *7*, 5523.

(12) Schauermann, S. Partial Hydrogenation of Unsaturated Carbonyl Compounds: Toward Ligand-Directed Heterogeneous Catalysis. *J. Phys. Chem. Lett.* **2018**, *9*, 5555.

(13) Mohr, C.; Hofmeister, H.; Lucas, M.; Claus, P. Gold Catalysts for the Partial Hydrogenation of Acrolein. *Chem. Eng. Technol.* **2000**, *23*, 324.

(14) Mohr, C.; Hofmeister, H.; Radnik, J.; Claus, P. Identification of Active Sites in Gold-Catalyzed Hydrogenation of Acrolein. *J. Am. Chem. Soc.* **2003**, *125*, 1905.

(15) Mohr, C.; Hofmeister, H.; Claus, P. The influence of real structure of gold catalysts in the partial hydrogenation of acrolein. *J. Catal.* **2003**, *213*, 86.

(16) Claus, P.; Brückner, A.; Mohr, C.; Hofmeister, H. Supported Gold Nanoparticles from Quantum Dot to Mesoscopic Size Scale: Effect of Electronic and Structural Properties on Catalytic Hydrogenation of Conjugated Functional Groups. *J. Am. Chem. Soc.* **2000**, *122*, 11430.

(17) Claus, P.; Hofmeister, H.; Mohr, C. Identification of Active Sites and Influence of Real Structure of Gold Catalysts in the Selective Hydrogenation of Acrolein to Allyl Alcohol. *Gold Bull.* **2004**, *37*, 181.

(18) Claus, P. Heterogeneously catalysed hydrogenation using gold catalysts. *Appl. Catal. A: General* **2005**, *291*, 222.

(19) Li, Z.; Chen, Z.-X.; He, X.; Kang, G.-J. Theoretical studies of acrolein hydrogenation on Au_{20} nanoparticle. *J. Chem. Phys.* **2010**, *132*, 184702.

(20) El-Roz, M.; Telegeiev, I.; Mordvinova, N. E.; Lebedev, O. I.; Barrier, N.; Behilil, A.; Zaarour, M.; Lakiss, L.; Valtchev, V. Uniform Generation of Sub-nanometer Silver Clusters in Zeolite Cages Exhibiting High Photocatalytic Activity under Visible Light. *ACS Appl. Mater. Interfaces* **2018**, *10*, 28702.

(21) Lee, S.; Molina, L. M.; López, M. J.; Alonso, J. A.; Hammer, B.; Lee, B.; Seifert, S.; Winans, R. E.; Elam, J. W.; Pellin, M. J.; Vajda, S. Selective Propene Epoxidation on Immobilized $Au_{6−−10}$ Clusters: The Effect of Hydrogen and Water on Activity and Selectivity. *Angew. Chem., Int. Ed.* **2009**, *48*, 1467.

(22) Vajda, S.; White, M. G. Catalysis Applications of Size-Selected Cluster Deposition. *ACS Catal.* **2015**, *5*, 7152.

(23) Halder, A.; Curtiss, L. A.; Fortunelli, A.; Vajda, S. Perspective: Size Selected Clusters for Catalysis and Electrochemistry. *J. Chem. Phys.* **2018**, *148*, 110901.

(24) Turner, M.; Golovko, V. B.; Vaughan, O. P. H.; Abdulkin, P.; Berenguer-Murcia, A.; Tikhov, M. S.; Johnson, B. F. G.; Lambert, R. M. Selective Oxidation with Dioxygen by Gold Nanoparticle Catalysts Derived from 55-atom Clusters. *Nature* **2008**, *454*, 981.

(25) *Protected Metal Clusters: From Fundamentals to Applications*; Tsukuda, T., Häkkinen, H., Eds.; Elsevier, Ltd., 2015.

(26) Xie, S.; Tsunoyama, H.; Kurashige, W.; Negishi, Y.; Tsukuda, T. Enhancement in Aerobic Alcohol Oxidation Catalysis of Au_{25} Clusters by Single Pd Atom Doping. *ACS Catal.* **2012**, *2*, 1519.

(27) Sudheeshkumar, V.; Sulaiman, K. O.; Scott, R. W. J. Activation of Atom-precise Clusters for Catalysis. *Nanoscale Adv.* **2020**, *2*, 55.

(28) Lopez-Acevedo, O.; Kacprzak, K. A.; Akola, J.; Häkkinen, H. Quantum Size Effects in Ambient CO Oxidation Catalysed by Ligand-protected Gold Clusters. *Nat. Chem.* **2010**, *2*, 329.

(29) Zhang, B.; Sels, A.; Salassa, G.; Pollitt, S.; Truttmann, V.; Rameshan, C.; Llorca, J.; Olszewski, W.; Rupprechter, G.; Bürgi, T.; Barrabés, N. Ligand Migration from Cluster to Support: A Crucial Factor for Catalysis by Thiolate-protected Gold Clusters. *ChemCatChem.* **2018**, *10*, 5372.

(30) Shen, H.; Deng, G.; Kaappa, S.; Tan, T.; Han, Y.-Z.; Malola, S.; Lin, S.-C.; Teo, B. K.; Häkkinen, H.; Zheng, N. Highly Robust but Surface-Active: An N-Heterocyclic Carbene-Stabilized Au_{25} Nanocluster. *Angew. Chemie. Int. Ed.* **2019**, *58*, 17731.

(31) Shen, H.; Xu, Z.; Hazer, M. S. A.; Wu, Q.; Peng, J.; Qin, R.; Malola, S.; Teo, B. K.; Häkkinen, H.; Zheng, N. Surface Coordination of Multiple Ligands Endows N-Heterocyclic Carbene-Stabilized Gold Nanoclusters with High Robustness and Surface Reactivity. *Angew. Chemie. Int. Ed.* **2021**, *60*, 3752.

(32) Lee, S.; Bootharaju, M. S.; Deng, G.; Malola, S.; Baek, W.; Häkkinen, H.; Zheng, N.; Hyeon, T. [Cu$_{32}$(PET)$_{24}$H$_8$Cl$_2$](PPh$_4$)$_2$: A Copper Hydride Nanocluster with a Bisquare Antiprismatic Core. *J. Am. Chem. Soc.* **2020**, *142*, 13974.

(33) Fang, J.; Zhang, B.; Yao, Q. F.; Yang, Y.; Xie, J. P.; Yan, N. Recent Advances in the Synthesis and Catalytic Applications of Ligand-Protected, Atomically Precise Metal Nanoclusters. *Coord. Chem. Rev.* **2016**, *322*, 1.

(34) Ansar, S. M.; Kitchens, C. L. Impact of Gold Nanoparticle Stabilizing Ligands on the Colloidal Catalytic Reduction of 4-Nitrophenol. *ACS Catal.* **2016**, *6*, 5553.

(35) Vu, K. B.; Bukhryakov, K. V.; Anjum, D. H.; Rodionov, V. O. Surface-Bound Ligands Modulate Chemoselectivity and Activity of a Bimetallic Nanoparticle Catalyst. *ACS Catal.* **2015**, *5*, 2529.

(36) Ackerson, C. J.; Jadzinsky, P. D.; Kornberg, R. D. Thiolate Ligands for Synthesis of Water-Soluble Gold Clusters. *J. Am. Chem. Soc.* **2005**, *127*, 6550.

(37) Dolamic, I.; Knoppe, S.; Dass, A.; Bürgi, T. First Enantioseparation and Circular Dichroism Spectra of Au$_{38}$ Clusters Protected by Achiral Ligands. *Nat. Commun.* **2012**, *3*, 798.

(38) Zhu, Y.; Wu, Z.; Gayathri, C.; Qian, H.; Gil, R. R.; Jin, R. Exploring stereoselectivity of Au$_{25}$ nanoparticle catalyst for hydrogenation of cyclic ketone. *J. Catal.* **2010**, *271*, 155.

(39) Tang, Q.; Lee, Y.; Li, D. Y.; Choi, W.; Liu, C. W.; Lee, D.; Jiang, D. E. Lattice-Hydride Mechanism in Electrocatalytic CO Reduction by Structurally Precise Copper-Hydride Nanoclusters. *J. Am. Chem. Soc.* **2017**, *139*, 9728.

(40) Sun, C.; Mammen, N.; Kaappa, S.; Yuan, P.; Deng, G.; Zhao, C.; Yan, J.; Malola, S.; Honkala, K.; Häkkinen, H.; Teo, B. K.; Zheng, N. Atomically Precise, Thiolated Copper—Hydride Nanoclusters as Single—Site Hydrogenation Catalysts for Ketones in Mild Conditions. *ACS Nano* **2019**, *13*, 5975.

(41) Cano, I.; Huertos, M. A.; Chapman, A. M.; Buntkowsky, G.; Gutmann, T.; Groszewicz, P. B.; van Leeuwen, P. W. N. M. Air-Stable Gold Nanoparticles Ligated by Secondary Phosphine Oxides as Catalyst for the Chemoselective Hydrogenation of Substituted Aldehydes: a Remarkable Ligand Effect. *J. Am. Chem. Soc.* **2015**, *137*, 7718.

(42) Almora-Barrios, N.; Cano, I.; van Leeuwen, P. W. N. M.; López, N. Concerted Chemoselective Hydrogenation of Acrolein on Secondary Phosphine Oxide Decorated Gold Nanoparticles. *ACS Catal.* **2017**, *7*, 3949.

(43) Azubel, M.; Kornberg, R. D. Synthesis of Water-Soluble, Thiolate-Protected Gold Nanoparticles Uniform in Size. *Nano Lett.* **2016**, *16*, 3348.

(44) Azubel, M.; Carter, S. D.; Weiszmann, J.; Zhang, J.; Jensen, G. J.; Li, Y.; Kornberg, R. D. FGF21 Trafficking in Intact Human Cells Revealed by Cryo-electron Tomography with Gold Nanoparticles. *eLife* **2019**, *8*, No. e43146.

(45) Azubel, M.; Koivisto, J.; Malola, S.; Bushnell, D.; Hura, G. L.; Koh, A. L.; Tsunoyama, H.; Tsukuda, T.; Pettersson, M.; Häkkinen, H.; Kornberg, R. D. Electron Microscopy of Gold Nanoparticles at Atomic Resolution. *Science* **2014**, *345*, 909.

(46) Azubel, M.; Koh, A. L.; Koyasu, K.; Tsukuda, T.; Kornberg, R. D. Structure Determination of a Water-Soluble 144-Gold Atom Particle at Atomic Resolution by Aberration-Corrected Electron Microscopy. *ACS Nano* **2017**, *11*, 11866.

(47) Tero, T.-R.; Malola, S.; Koncz, B.; Pohjolainen, E.; Lautala, S.; Mustalahti, S.; Permi, P.; Groenhof, G.; Pettersson, M.; Häkkinen, H. Dynamic Stabilization of the Ligand—Metal Interface in Atomically Precise Gold Nanoclusters Au$_{68}$ and Au$_{144}$ Protected by meta-Mercaptobenzoic Acid. *ACS Nano* **2017**, *11*, 11872.

(48) Black, D. M.; Hoque, M. M.; Plascencia-Villa, G.; Whetten, R. L. New Evidence of the Bidentate Binding Mode in 3-MBA Protected Gold Clusters: Analysis of Aqueous 13−18 kDa Gold-Thiolate Clusters by HPLC-ESI-MS Reveals Special Compositions Au$_n$(3-MBA)$_p$, (n = 48−67, p = 26−30). *Nanomaterials* **2019**, *9*, 1303.

(49) Mammen, N.; Malola, S.; Honkala, K.; Häkkinen, H. Dynamics of Weak Interactions in the Ligand Layer of *meta*-Mercaptobenzoic

Acid Protected Gold Nanoclusters Au$_{68}$(*m*-MBA)$_{32}$ and Au$_{144}$(*m*-MBA)$_{40}$. *Nanoscale* **2020**, *12*, 23859.

(50) Enkovaara, J; Rostgaard, C; Mortensen, J J; Chen, J; Dułak, M; Ferrighi, L; Gavnholt, J; Glinsvad, C; Haikola, V; Hansen, H A; Kristoffersen, H H; Kuisma, M; Larsen, A H; Lehtovaara, L; Ljungberg, M; Lopez-Acevedo, O; Moses, P G; Ojanen, J; Olsen, T; Petzold, V; Romero, N A; Stausholm-Møller, J; Strange, M; Tritsaris, G A; Vanin, M; Walter, M; Hammer, B; Hakkinen, H; Madsen, G K H; Nieminen, R M; Nørskov, J K; Puska, M; Rantala, T T; Schiøtz, J; Thygesen, K S; Jacobsen, K W Electronic Structure Calculations with GPAW: A Real-Space Implementation of the Projector Augmented-Wave Method. *J. Condens. Matter Phys.* **2010**, *22*, 253202.

(51) Perdew, J. P.; Burke, K.; Ernzerhof, M. Generalized Gradient Approximation Made Simple. *Phys. Rev. Lett.* **1996**, *77*, 3865.

(52) Narouz, M. R.; Takano, S.; Lummis, P. A.; Levchenko, T. I.; Nazemi, A.; Kaappa, S.; Malola, S.; Yousefalizadeh, G.; Calhoun, L. A.; Stamplecoskie, K. G.; Häkkinen, H.; Tsukuda, T.; Crudden, C. M. Robust, Highly Luminescent Au$_{13}$ Superatoms Protected by N-Heterocyclic Carbenes. *J. Am. Chem. Soc.* **2019**, *141*, 14997.

(53) Tkatchenko, A.; Scheffler, M. Accurate Molecular Van Der Waals Interactions from Ground-State Electron Density and Free-Atom Reference Data. *Phys. Rev. Lett.* **2009**, *102*, 073005.

(54) Ruiz, V. G.; Liu, W.; Tkatchenko, A. Density-functional theory with screened van der Waals interactions applied to atomic and molecular adsorbates on close-packed and non-close-packed surfaces. *Phys. Rev. B* **2016**, *93*, 035118.

(55) Ruiz, V. G.; Liu, W.; Zojer, E.; Scheffler, M.; Tkatchenko, A. Density-Functional Theory with Screened van der Waals Interactions for the Modeling of Hybrid Inorganic-Organic Systems. *Phys. Rev. Lett.* **2012**, *108*, 146103.

(56) Wang, Y.; Verma, P.; Jin, X.; Truhlar, D. G.; He, X. Revised M06 density functional for main-group and transition-metal chemistry. *Proc. Natl. Acad. Sci. U. S. A.* **2018**, *115*, 10257.

(57) Bajdich, M.; Nørskov, J. K.; Vojvodic, A. Surface energetics of alkaline-earth metal oxides: Trends in stability and adsorption of small molecules. *Phys. Rev. B* **2015**, *91*, 155401.

(58) Falsig, H.; Hvolbæk, B.; Kristensen, I. S.; Jiang, T.; Bligaard, T.; Christensen, C. H.; Nørskov, J. K. Trends in the Catalytic CO Oxidation Activity of Nanoparticles. *Angew. Chemie. Int. Ed.* **2008**, *120*, 4913.

(59) Malone, W.; Matos, J.; Kara, A. Adsorption of Thiophene on Transition Metal Surfaces with the Inclusion of van der Waals Effects. *Surf. Sci.* **2018**, *669*, 121.

(60) Freire, R. L. H.; Guedes-Sobrinho, D.; Kiejna, A.; Da Silva, J. L. F. Comparison of the Performance of van der Waals Dispersion Functionals in the Description of Water and Ethanol on Transition Metal Surfaces. *J. Phys. Chem. C* **2018**, *122*, 1577.

(61) Barmparis, G. D.; Honkala, K.; Remediakis, I. N. Thiolate adsorption on Au(hkl) and equilibrium shape of large thiolate-covered gold nanoparticles. *J. Chem. Phys.* **2013**, *138*, 064702.

(62) Akola, J.; Walter, M.; Whetten, R.; Häkkinen, H.; Grönbeck, H. On the structure of thiolate-protected Au$_{25}$. *J. Am. Chem. Soc.* **2008**, *130*, 3756.

(63) Lopez-Acevedo, O.; Tsunoyama, H.; Tsukuda, T.; Häkkinen, H.; Aikens, C. M. Chirality and electronic structure of the thiolate-protected Au38 nanocluster. *J. Am. Chem. Soc.* **2010**, *132*, 8210.

(64) Lopez-Acevedo, O.; Akola, J.; Whetten, R.; Grönbeck, H.; Häkkinen, H. Structure and Bonding in the Ubiquitous Icosahedral Metallic Gold Cluster Au$_{144}$(SR)$_{60}$. *J. Phys. Chem. C* **2009**, *113*, 5035.

(65) Heaven, M. W.; Dass, A.; White, P. S.; Holt, K. M.; Murray, R. W. Crystal Structure of the Gold Nanoparticle [N(C$_8$H$_{17}$)$_4$]-[Au$_{25}$(SCH$_2$CH$_2$Ph)$_{18}$]. *J. Am. Chem. Soc.* **2008**, *130*, 3754.

(66) Qian, H.; Eckenhoff, W. T.; Zhu, Y.; Pintauer, T.; Jin, R. Total Structure Determination of Thiolate-Protected Au$_{38}$ Nanoparticles. *J. Am. Chem. Soc.* **2010**, *132*, 8280.

(67) Yan, N.; Xia, N.; Liao, L.; Zhu, M.; Jin, F.; Jin, R.; Wu, Z. Unraveling the long-pursued Au$_{144}$ structure by x-ray crystallography. *Sci. Adv.* **2018**, *4*, aat7259.

(68) Cao, Y.; Malola, S.; Matus, M. F.; Chen, T.; Yao, Q.; Shi, R.; Häkkinen, H.; Xie, J. Reversible isomerization of metal nanoclusters induced by intermolecular interaction. *Chem.* **2021**, *7*, 2227.

(69) Malola, S.; Häkkinen, H. Chiral Inversion of Thiolate-Protected Gold Nanoclusters via Core Reconstruction without Breaking an Au-S Bond. *J. Am. Chem. Soc.* **2019**, *141*, 6006.

(70) Henkelman, H.; Uberuaga, B. P.; Jónsson, H. A Climbing Image Nudged Elastic Band Method for Finding Saddle Points and Minimum Energy Paths. *J. Chem. Phys.* **2000**, *113*, 9901.
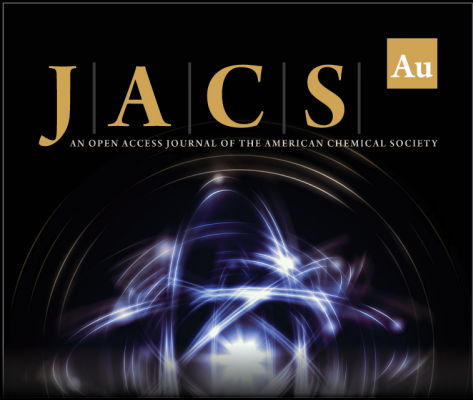
(71) Kaduk, B.; Kowalczyk, T.; Van Voorhis, T. Constrained Density Functional Theory. *Chem. Rev.* **2012**, *112*, 321.

(72) Malola, S.; Nieminen, P.; Pihlajamäki, A.; Hämäläinen, J.; Kärkkäinen, T.; Häkkinen, H. A Method for Structure Prediction of Metal-ligand Interfaces of Hybrid Nanoparticles. *Nat. Commun.* **2019**, *10*, 3973.

(73) Fiorio, J. L.; López, N.; Rossi, L. M. Gold-Ligand-Catalyzed Selective Hydrogenation of Alkynes into *cis-* Alkenes via H_2 Heterolytic Activation by Frustrated Lewis Pairs. *ACS Catal.* **2017**, *7*, 2973.

(74) Yang, X.; Wang, A.; Wang, X.; Zhang, T.; Han, K.; Li, J. Combined Experimental and Theoretical Investigation on the Selectivities of Ag, Au, and Pt Catalysts for Hydrogenation of Crotonaldehyde. *J. Phys. Chem. C* **2009**, *113*, 20918.

(75) He, X.; Chen, Z.-X.; Kang, G.-J. Theoretical Study of the Role of Indium on the Selectivity of Acrolein Hydrogenation to Propenol on Gold Surfaces. *J. Phys. Chem. C* **2009**, *113*, 12325.